Electronic Supplementary Material

Cobalt nitride enabled benzimidazoles production from furyl/aryl bio-alcohols and *o*-nitroanilines without an external H-source

Chuanhui Li, Li-Long Zhang, Hu Li **(✉)**, Song Yang **(✉)**

State Key Laboratory Breeding Base of Green Pesticide & Agricultural Bioengineering, Key Laboratory of Green Pesticide & Agricultural Bioengineering, Ministry of Education, State-Local Joint Laboratory for Comprehensive Utilization of Biomass, Center for R&D of Fine Chemicals, Guizhou University, Guiyang 550025, China

E-mails: hli13@gzu.edu.cn (Li H); jhzx.msm@gmail.com (Yang S)

1. Experimental

1.1. Material

Cobalt nitrate hexahydrate ($Co(NO_3)_2·6H_2O$, 99%), 1,4-dioxane (99%), and furfural (FUR, 99%) were purchased from Chengdu Jinshan Chemical Reagent Factory. Methanol (MeOH, 99%), ethanol (EtOH, 99%), tetrahydrofuran (THF, 99%), acetonitrile (CH_3CN, 99%), dichloromethane (DCM, 99%), cyclohexane (CYH, 99%), chlorobenzene (PhCl, 99%), toluene (99%) and *N,N*-dimethylformamide (DMF, 99%) were purchased from Tianjin Fuyu Fine Chemicals Co., Ltd. Dimethyl sulfoxide (DMSO, 99%), acetophenone (99%), hydrochloric acid (HCl, 12%) and naphthalene (99%) were purchased from Shanghai Aladdin Reagent Co. Zinc nitrate hexahydrate ($Zn(NO_3)_2·6H_2O$, 99%) and potassium thiocyanate (KSCN, 99%) were purchased from Beijing Alfa Aesar Chemical Co., Ltd. Terephthalic acid (99%) was purchased from Shanghai Energy Chemical. Benzaldehyde, all *o*-nitroanilines, alcohols, and benzimidazoles were purchased from Aladdin Reagent Co., Ltd. (Shanghai, China).

1.2. Catalyst preparation

Synthesis of ZIF-67: ZIF-67 precursors were prepared in different solvents by stirring at room temperature. In a typical procedure, 2-methylimidazole (8 mmol) was first added into 40 mL of methanol contained in a 100 beaker, followed by transfer into an oil bath (25 °C) and stirring until complete dissolution to obtain solution A. Afterward, 20 mL of $Co(NO_3)_2·6H_2O$ (1 mmol) dissolved in methanol was dropwise added into the solution A, followed by stirring for 0.5 h, and then kept for 24 h at 25 °C. Upon completion, the bright purple product was collected by filtration, washed 3 times with methanol, and dried at 60 °C under vacuum for 12 h. In addition, solvent like water or ethanol with triethylamine was also used for the preparation of ZIF-67 to explore the influence of alkali and different solvation on the morphology of ZIF-67. The preparation procedures are the same as above except for adding triethylamine and other solvents instead of methanol.

Synthesis of ZIF-8: The ZIF-8 precursor was synthesized according to the reported synthesis method. Briefly, $Zn(NO_3)_2·6H_20$ (0.6 g) was dissolved into 50 mL

of deionized water. Then, 37 mL of 2-methylimidazole (2.6 g) aqueous solution was added into the above mixture and stirred vigorously at 80 °C for 12 h. The white mixture was centrifuged, and the resulting white solid was washed with methanol three times and then dried overnight at 80 °C.

Synthesis of MOF-71: MOF-71 was prepared based on previous literature with minor changes. $Co(NO_3)_2 \cdot 6H_2O$ (0.75 g) and terephthalic acid (0.425 g) were dissolved into DMF (48 mL) and absolute EtOH (12 mL). The resulting mixture solution was violently stirred at room temperature for 1 h, and then transferred into a 100 mL polytetrafluoroethylene (PTFE) kettle and placed into an oven at 110 °C aging for 12 h. After cooling to room temperature, MOF-71 was obtained by centrifuge, washing three times with methanol, and drying in a vacuum oven at 80 °C overnight.

1.3. Catalyst characterization

Field emission scanning electron microscopy (SEM, FEI Nova NanoSEM 450) was used to observe the morphology and shape of the catalyst. The structure and the element mapping were analyzed by a high-resolution transmission electron microscope (HR-TEM, FEI Tecnai G2 F20) with EDX analysis (Bruker Xflash 5030T) operating at 300 kV. In order to understand the distribution of atoms inside the catalyst, the X-ray diffraction (XRD) analysis of catalysts was carried out in a Bruker Advanced D8 Powder Diffractometer using Cu Kα radiation source in the wide-angle diffraction range (2θ = 10-80°). To examine the changes of the internal physical structure of ZIF-67 precursor before and after calcination, N_2 adsorption-desorption measurements of the catalysts were carried out on the Micromeritics ASAP 2010 instrument at 77K. Thermogravimetric (TG) analysis was conducted by Shimadzu DTG-60 AH differential thermal analyzer with the temperature ranging from room temperature to 800 °C. Raman spectra were collected on Confocal Laser Micro-Raman Spectrometer (Thermo Fisher DXR 2XI). X-ray photoelectron spectroscopy (XPS) testing of the catalyst was performed on the Escalab 250Xi Spectrometer to analyze the composition of the catalyst surface.

NH_3-TPD patterns of catalysts were carried out on a Micromeritics AutoChem Π 2920 chemical adsorption analyzer with a He flow of 20 mL/min (10 vol% NH_3). The alkalinity of the catalyst was measured by carbon dioxide temperature program desorption (CO_2-TPD) on the AutoChem 2920 chemical adsorption analyzer with a He flow of 20 mL/min (10 vol% CO_2). Inductively coupled plasma optical emission spectrometry (ICP-OES) was employed to analyze the Co content in the obtained Co/CN_x-T samples.

1.4. The analytical methods of GC and GC-MS

Products analysis was performed on an Agilent 7890A gas chromatography (GC) instrument with a crosslinked capillary DB-5 column (30 m × 0.320 mm × 0.25 μm) equipped with a flame ionization detector (FID). Operating conditions were as follows: The flow rate of the N_2 carrier gas was 0.8 mL min^{-1}, and the injection port temperature was 270 °C. The GC oven temperature program was as follows: 60 °C at a rate of 10 °C/min to 230 °C, hold for 5 minutes. The detector temperature was set at 270 °C. Naphthalene was used as the internal standard to determine the content of each compound.

The structure of the compound was determined by gas chromatography-mass spectrometry (GC-MS Agilent 6890N GC/5973 MS) with a crosslinked capillary DB-5 column (30 m × 0.320 mm × 0.25 μm). The flow rate of the He carrier gas was 0.8 mL min^{-1}, and the injection port temperature was 280 °C. The GC oven temperature program was as follows: 60 °C at a rate of 10 °C/min to 290 °C, and hold for 5 min.

1.5. Calculation method

Density functional theory (DFT) calculations were all done with the Gaussian 16 suite.[S1] Geometry optimization and frequency calculation were carried out with the B3LYP method, In this paper, the optimized structures and harmonic vibrational frequency calculations were used with a 6-31G(d) basis set for H, C, O, and LANL2DZ basis set for Co. To more accurately access the electronic energies, single-point energy calculations were performed at the same function with diffusion

6-31+G(d,p) basis set for H, C, O, and SDD pseudopotential basis set for Co atom.

Supplementary Tables

Table S1 Comparison of various catalyst activities in the synthesis of benzimidazoles from alcohols and *o*-nitrobenzenes.

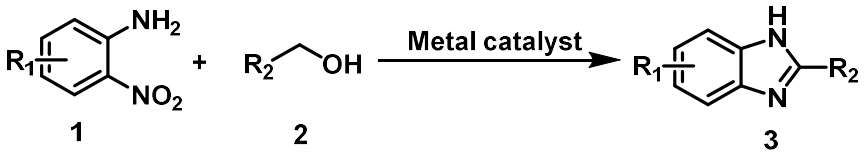

1 2 3

Catalyst	Base	Solvent	Temperature	Time	Inert gases	Yield of 3	Ref.
Non-noble metal catalysts							
Co/CN_x-700		cyclohexane	150 °C	10 h		65%~92%	This work
$Co(acac)_2$	^{t}BuONa	1,4-dioxane	135 °C	24 h	Ar	36%~81%	[S2]
Dppf		toluene	150 °C	24 h	Ar	40%~88%	[S3]
Fe catalyst	^{t}BuONa	PhCl	150 °C	42 h		59%~80%	[S4]
$NaS{\cdot}nH_2O+FeCl_3{\cdot}6H_20$			140 °C	24	Ar	44%-98%	[S5]
Cu-Zn-PMO			250 °C	6 h		78%~90%	[S6]
Noble-metal catalysts							
Ir/TiO_2		mesitylene	80 °C	18 h	Ar	22%~99%	[S7]
Pd/C	^{t}BuOK	PhCl	80 °C	4 h	N_2	49%~99%	[S8]
Ir/TiO_2		mesitylene	120 °C	18 h	Ar	93%	[S9]
Au/TiO_2		toluene	150 °C	24 h	N_2	78%	[S10]
Pd/HT		toluene	160 °C	48 h	N_2	96%	[S11]
Cu–Pd/γ-Al_2O_3		H_2O	180 °C	12 h	N_2	5.8%~100%	[S12]

Table S2 Textural parameters of various samples investigated in this work

Entry	Sample	S_{BET} [a] [m^2 g^{-1}]	S_{micro} [b] [m^2 g^{-1}]	S_{meso} [c] [m^2 g^{-1}]	V_{total} [d] [cm^3 g^{-1}]	V_{micro}/V_{meso} [e] [cm^3 g^{-1}]	Pore size [f] (nm)
1	ZIF-67	2444	2244	200	1.34	1.10/0.24	2.2
2	Co/CN_x-600	228	109	119	0.25	0.05/0.20	4.3
3	Co/CN_x-700	334	86	248	0.34	0.05/0.29	4.1
4	Co/CN_x-800	329	57	272	0.39	0.03/0.36	4.7
5	Co/CN_x-900	206	71.0	135	0.26	0.06/0.20	3.9
6[g]	Co/CN_x-700^2	102	27	75	0.16	0.01/0.15	6.2
7[h]	Co/CN_x-700(ac)^2	276	91	185	0.31	0.05/0.26	4.4

[a] S_{BET} is the specific surface area calculated by the multipoint BET method. [b] S_{micro} is the specific surface area of micropores calculated by t-plot method. [c] S_{meso} is the surface area of mesopores calculated by S_{BET}–S_{micro}. [d] V_{total} is the total specific pore volume determined by using the adsorption branch of the N_2 isotherm at P/Po=0.99. [e] V_{micro} is the specific pore volume of micropores determined by the t-plot method and V_{meso} is the specific pore volume of mesopores calculated by V_{total}–V_{micro}. [f] Pore size is the adsorption average pore diameter by BET. [g] Three unactivated catalysts were used consecutively. [h]The activated catalyst was used thrice.

Table S3 Co 2p, C 1s, and N 1s components of different samples collected from XPS

Catalyst	Element content (at%)					Relative content of the Co, N species (%)				
	Co	N	C	O	Co^0	Co-N_x	Pyridinic N	Co-N_x	Pyrrolic N	Graphitic N
Co/CN_x-600	3.59	12.63	74.59	9.18	10.9	18.6	34.3	29.9	16.1	19.5
Co/CN_x-700	2.54	7.87	81.21	8.38	18.0	18.0	33.3	28.4	15.9	22.4
Co/CN_x-800	2.63	6.86	82.81	7.76	20.3	19.7	30.2	24.6	15.3	29.9
Co/CN_x-700(ac)^2	1.83	6.03	86.36	5.78	24.7	17.9	36.2	27.4	18.3	18.1

Table S4 ICP-OES analysis of Co content in the as-prepared Co/CN_x-T and Co/CN_x-700(ac)[2].

Entry	Sample	Element	Metal Content (wt%)
1	Co/CN_x-600	Co	29.9
2	Co/CN_x-700	Co	32.8
3	Co/CN_x-800	Co	35.9
4	Co/CN_x-900	Co	40.8
5	Co/CN_x-700(ac)[2]	Co	32.6

Table S5 Influence of solvent type on the synthesis of **3a** [a].

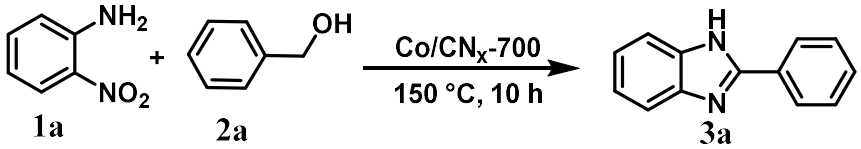

Entry	Solvent	Conv. of **1a**/(%)[b]	Yield of **3a**/(%)[b]	Select. of **3a**/(%)
1	**Cyclohexane**	**99**	**85.8**	**86.6**
2	**Toluene**	**99**	**84.0**	**84.9**
3	**Chlorobenzene**	**99**	**87.4**	**88.2**
4	Dichloromethane	35.3	12.5	35.4
5	Tetrahydrofuran	42.0	27.9	66.4
6	1,4-Dioxane	42.0	13.8	30.2
7	Acetonitrile	81.2	68.0	83.8
8	N,N-Dimethylformamide	81.5	59.8	73.3
9	Dimethyl sulfoxide	48.7	17.5	36.9

[a] Reaction conditions: **1a** (0.5 mmol), **2a** (1.5 mmol), Co/CN_x-700 (30 mg), solvent (2 mL), 150 °C, 10 h. [b] Conversion and yield were determined by GC. **1a**: *o*-nitroaniline; **2a**: benzyl alcohol; **3a**: 2-phenylbenzimidazole.

Table S6 Different catalysts for the conversion of *o*-nitroaniline (**1a**) and benzyl alcohol (**2a**) to 2-phenylbenzimidazole (**3a**) [a].

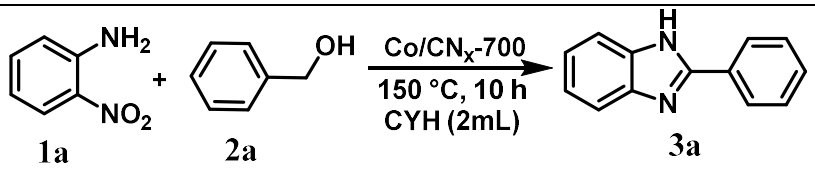

1a 2a 3a

Entry	Catalyst	Conv. of **1a**/(%)[b]	Yield of **3a**/(%)[b]	Select. of **3a**/(%)
1	AC[c]	12	2.3	20
2	NC-700[d]	6.3	2.7	43
3	Co/C-700[e]	19	13	68
4	CoO_x/NC-700[f]	8.3	5.6	67
5	Co/CN_x-700(HCl)[g]	81	60	74
6	Co/CN_x-700+KSCN[h]	33	29	88

[a] Reaction conditions: **1a** (0.5 mmol), **2a** (1.5 mmol), catalyst (30 mg), cyclohexane (2 mL), 150 °C, 10 h. [b] Conversion and yield were determined by GC. [c] Activated carbon; [d] Obtained from the pyrolysis of ZIF-8; [e] Obtained from the pyrolysis of MOF-71; [f] Obtained by calcination of ZIF-67 in the air at 700 °C; [g] Obtained by acid washing to remove the Co NPs while still preserving the Co-N_x; [h] 1 mmol KSCN was added.

Supplementary Figures

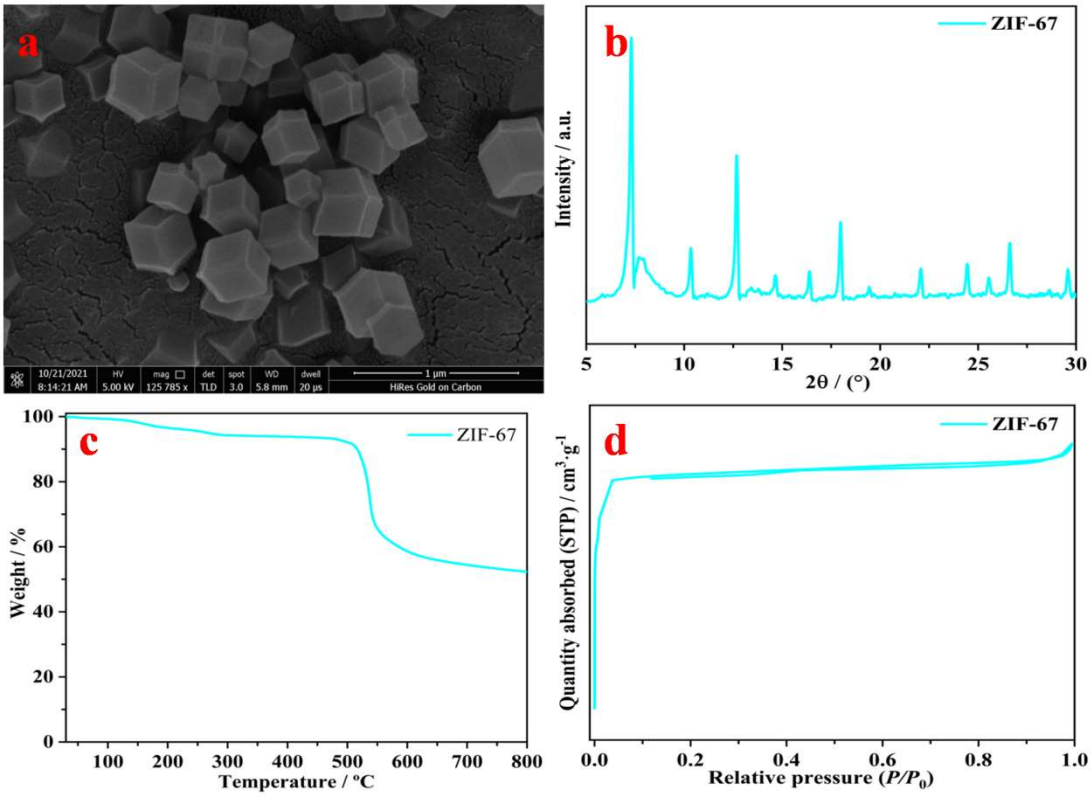

Fig. S1 a) SEM image of ZIF-67; b) XRD pattern of ZIF-67; c) Thermogravimetric analysis of ZIF-67; and d) N_2 adsorption-desorption isotherm of ZIF-67.

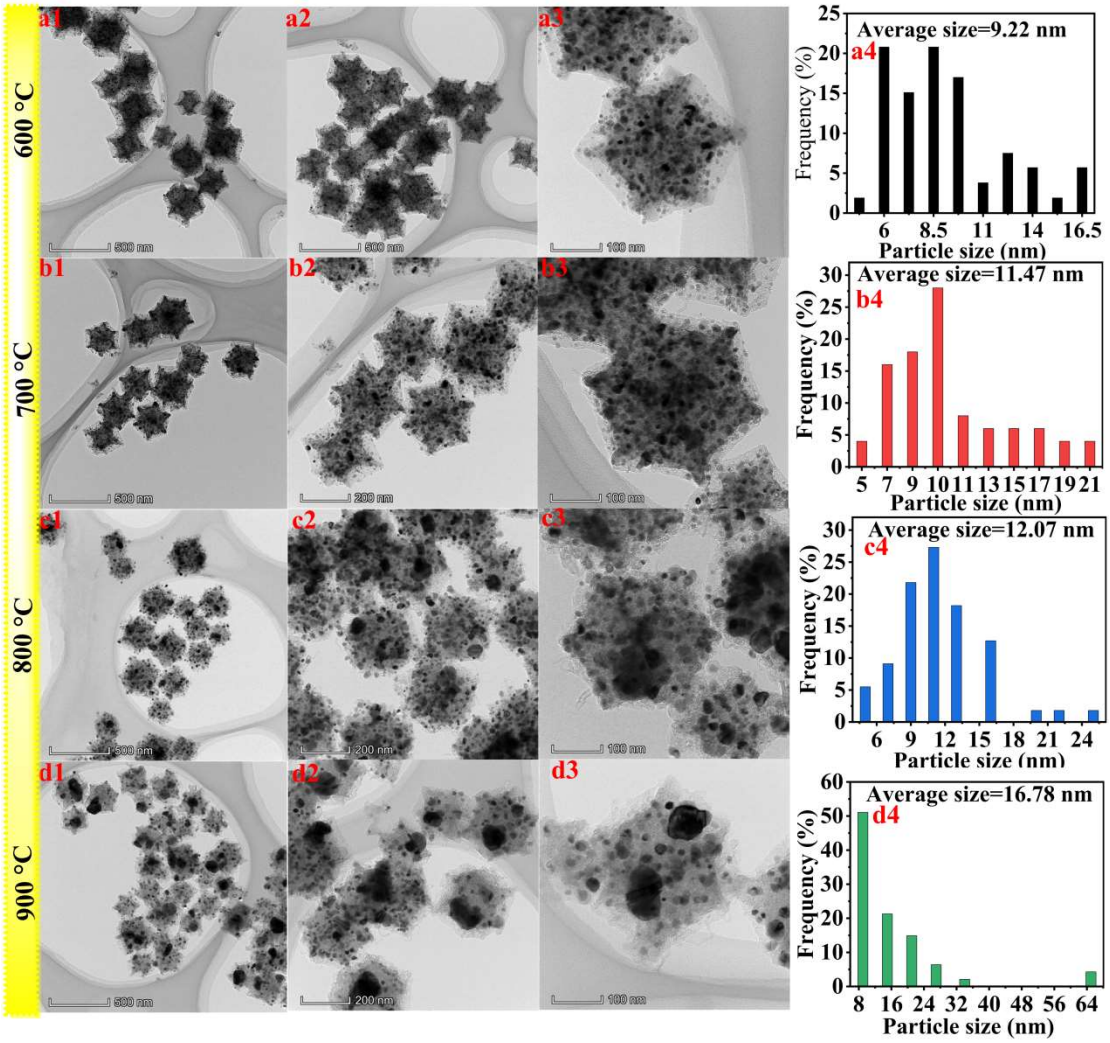

Fig. S2 The HR-TEM images and particle size distribution of cobalt nanoparticles of Co/CN_x-T (T = 600, 700, 800, 900 °C).

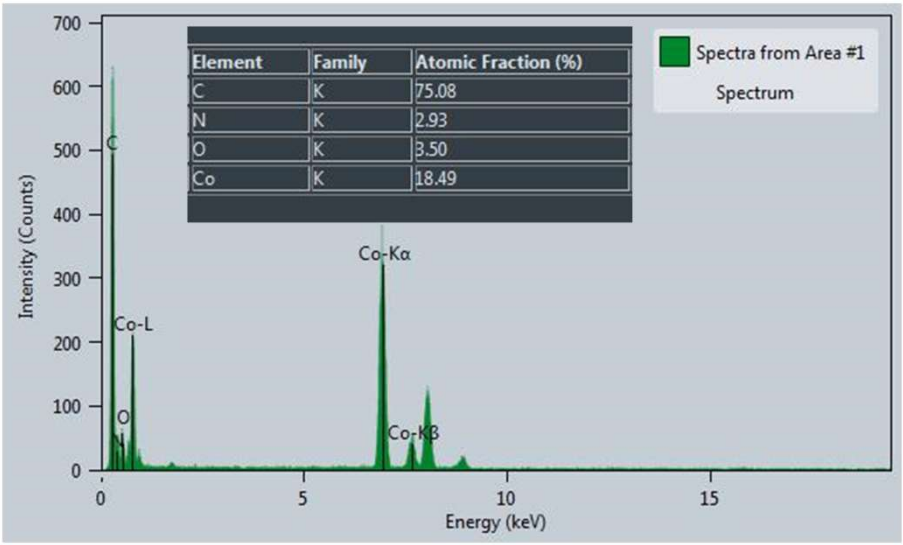

Fig. S3 EDS spectrum of Co/CN_x-700.

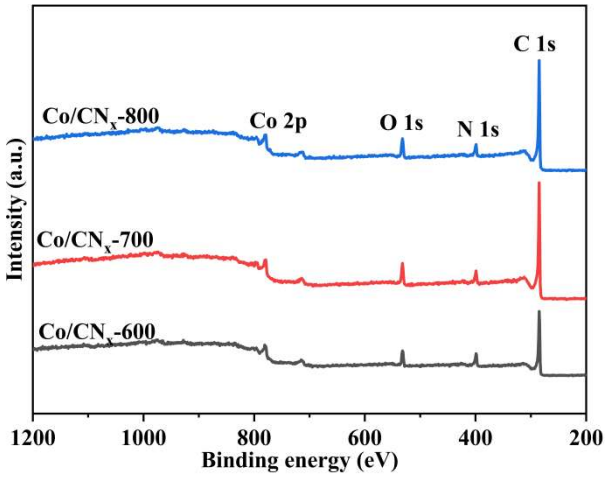

Fig. S4 Wide-range XPS spectra of Co/CN_x-T.

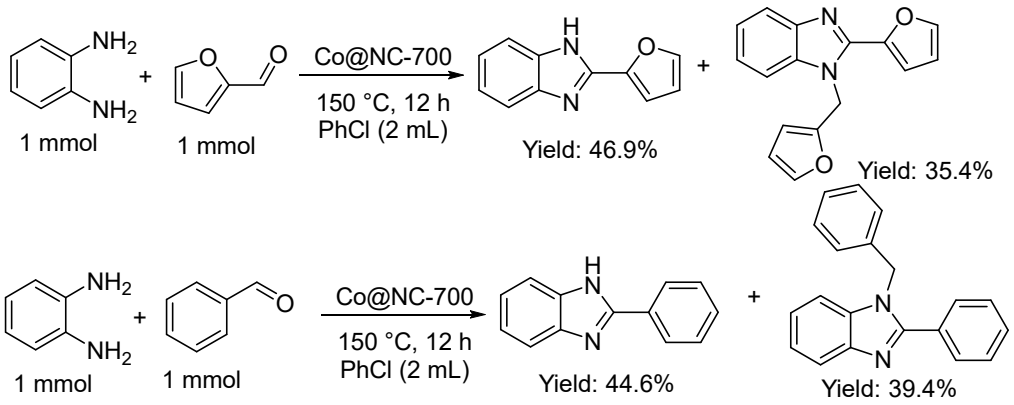

Fig. S5 Co/CN_x-700-catalyzed formation of 2-substituted and 1,2-disubstituted benzimidazoles from *o*-phenylenediamine and biomass aldehydes.

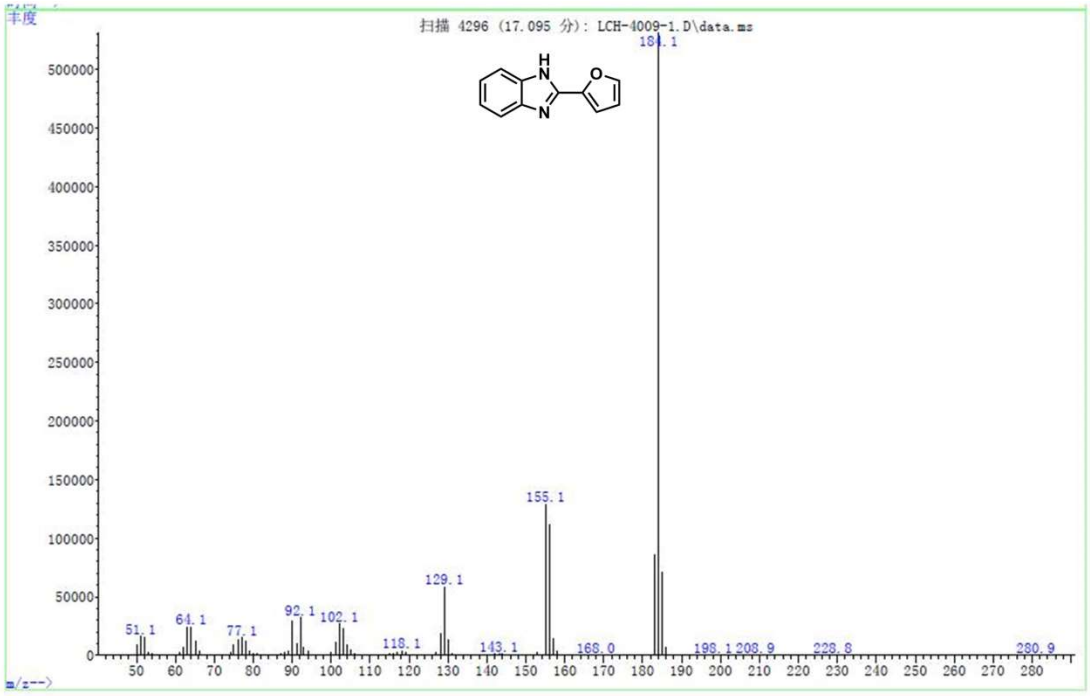

Fig. S6 MS spectrum of 2-(2-furanyl)-1*H*-Benzimidazole: abundance and m/z, scan (4296), 17.095 min.

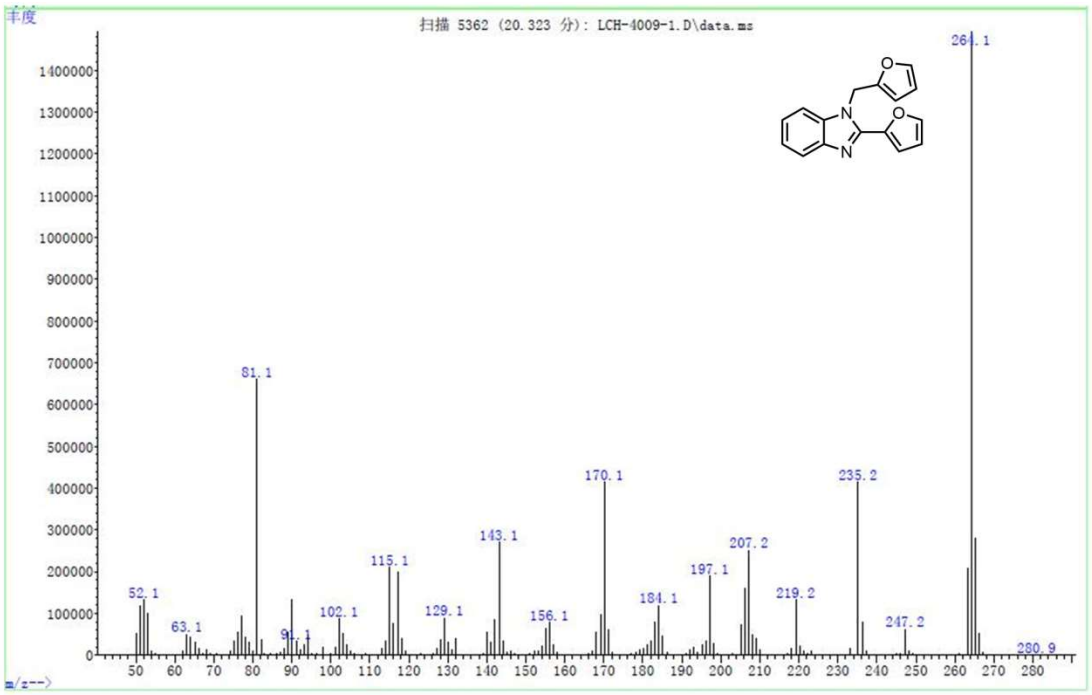

Fig. S7 MS spectrum of 2-(2-furanyl)-1-(2-furanylmethyl)-1*H*-Benzimidazole: abundance and m/z, scan (5362), 20323 min.

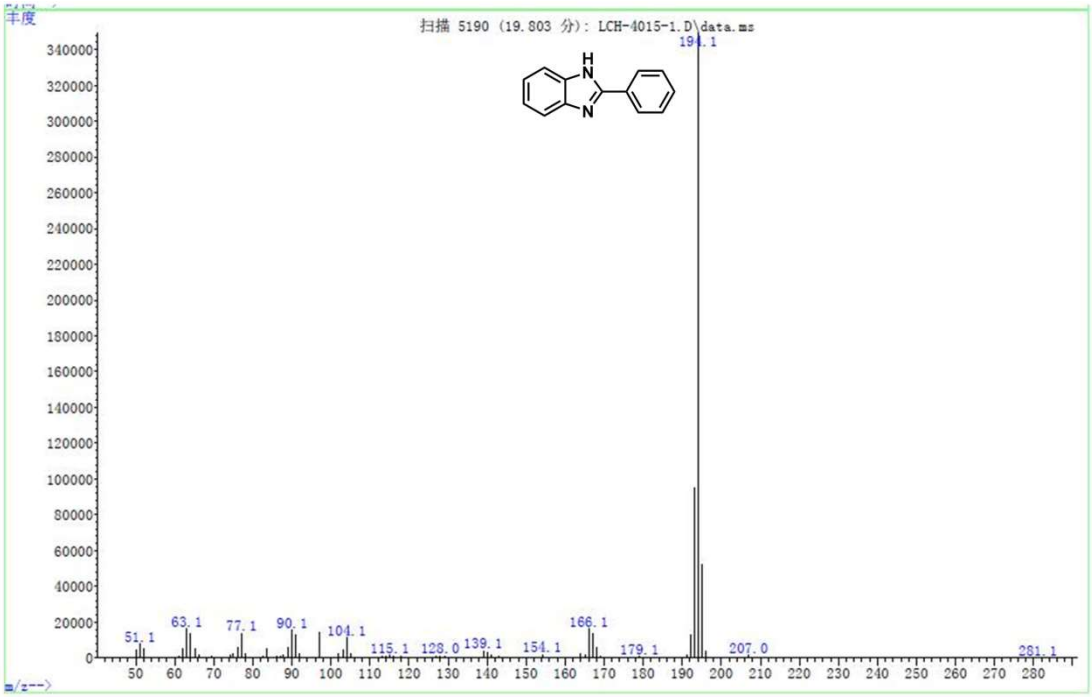

Fig. S8 MS spectrum of 2-phenyl-1*H*-Benzimidazole: abundance and m/z, scan (5190), 19.503 min.

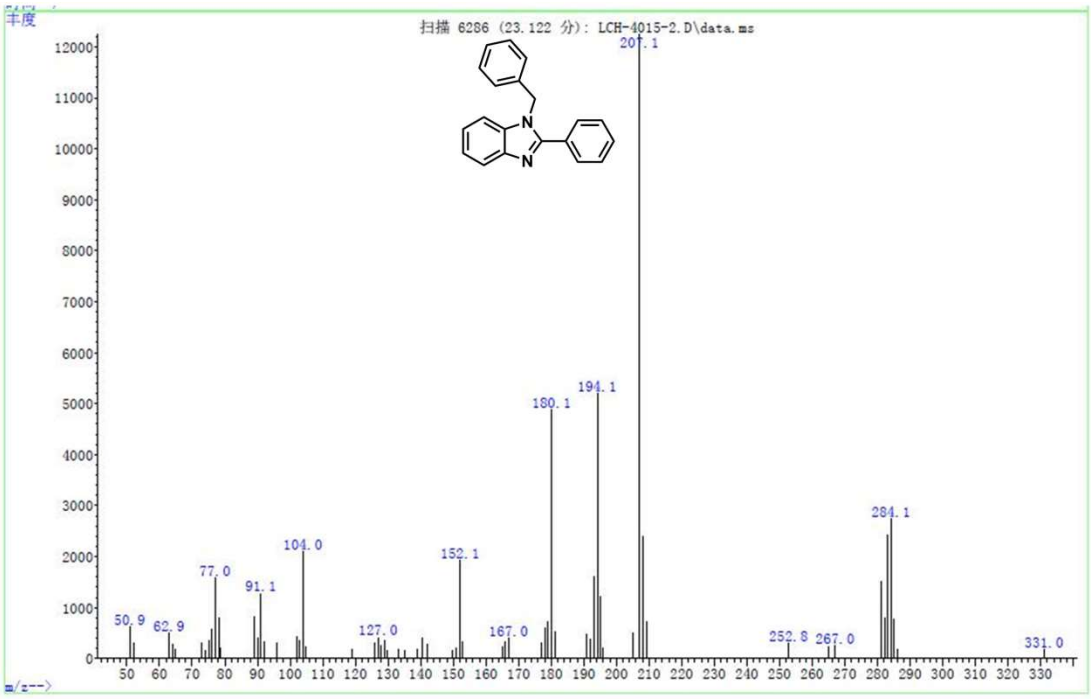

Fig. S9 MS spectrum of 2-phenyl-1-(phenylmethyl)-1*H*-Benzimidazole: abundance and m/z, scan (6286), 23.122 min.

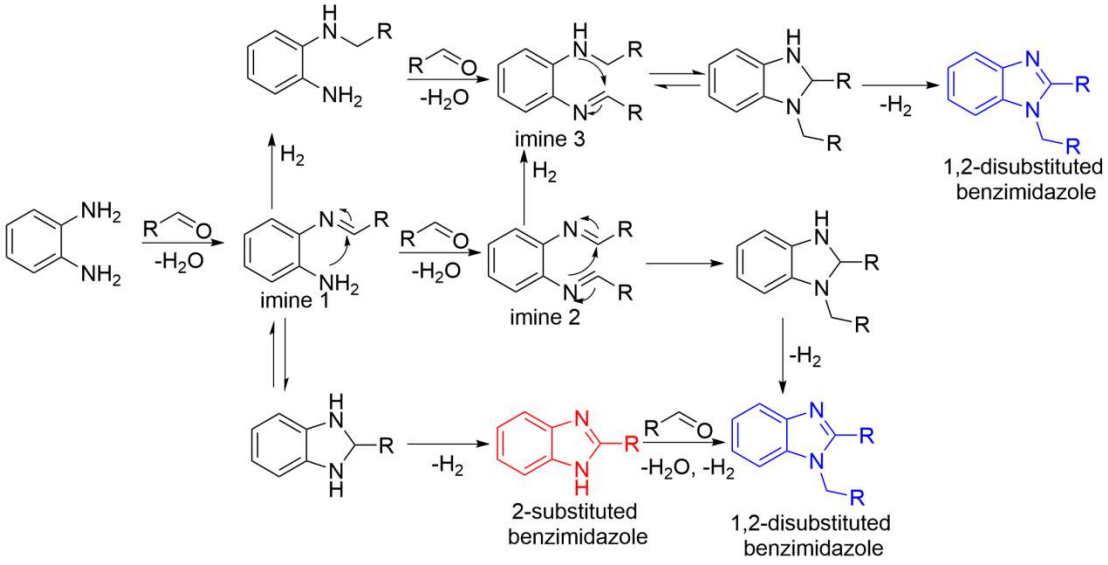

Fig. S10 Proposed reaction network for the formation of 2-substituted and 1,2-disubstituted benzimidazole from *o*-phenylenediamine and biomass aldehydes.

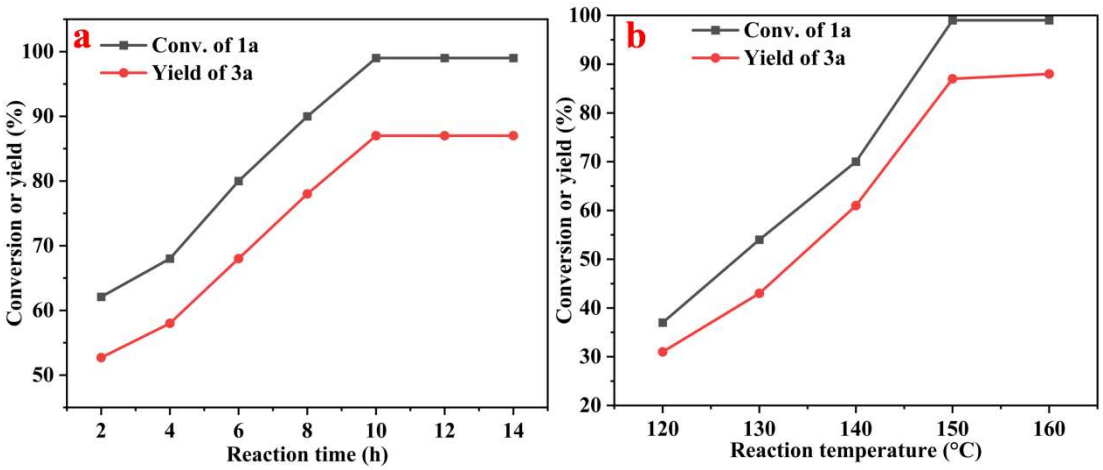

Fig. S11 The effect of reaction time (a), and reaction temperature (b) on the reaction. Reaction conditions: **1a** (0.5 mmol), **2a** (1.5 mmol), PhCl (2 mL), Co/CN_x-700 (0.03 g). **1a**: o-nitroaniline; **3a**: 2-phenylbenzimidazole.

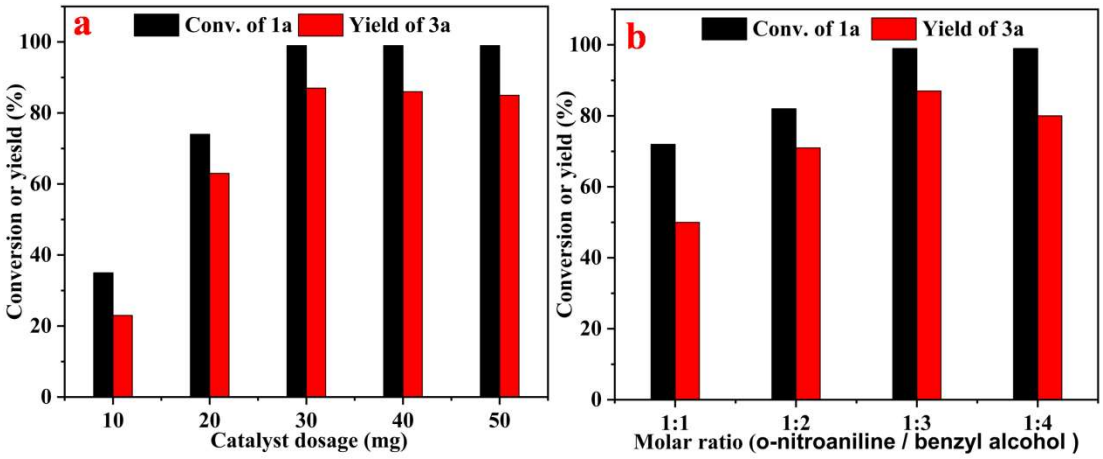

Fig. S12 The influence of the catalyst amount (a), and substrate molar ratio (b) on the reaction. Reaction conditions: **1a** (0.5 mmol), **2a** (1.5 mmol), PhCl (2mL), 150 °C, 10 h. **1a**: o-nitroaniline; **3a**: 2-phenylbenzimidazole.

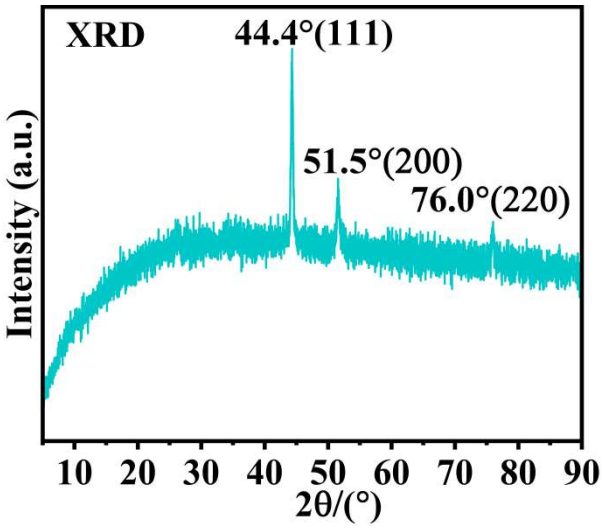

Fig. S13 The XRD pattern of Co/C-700.

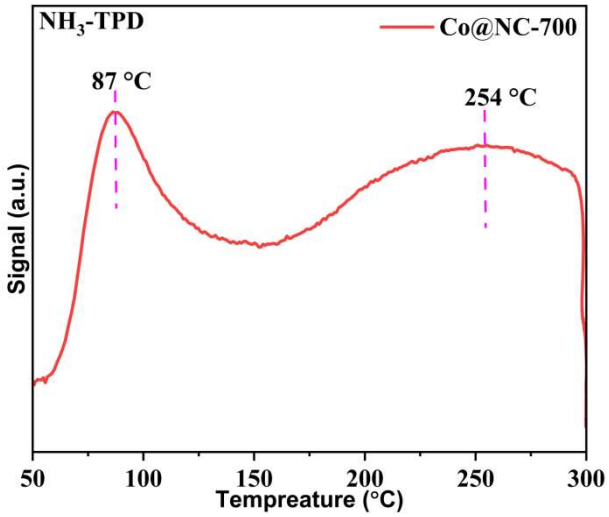

Fig. S14 NH_3-TPD spectrum of the obtained Co/CN_x-700 materials.

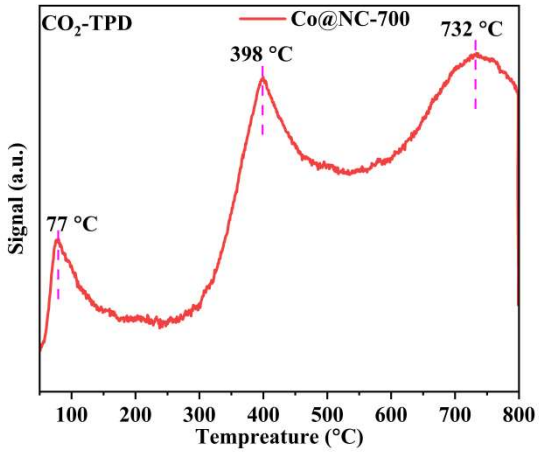

Fig. S15 CO_2-TPD spectrum of the obtained Co/CN_x-700 materials.

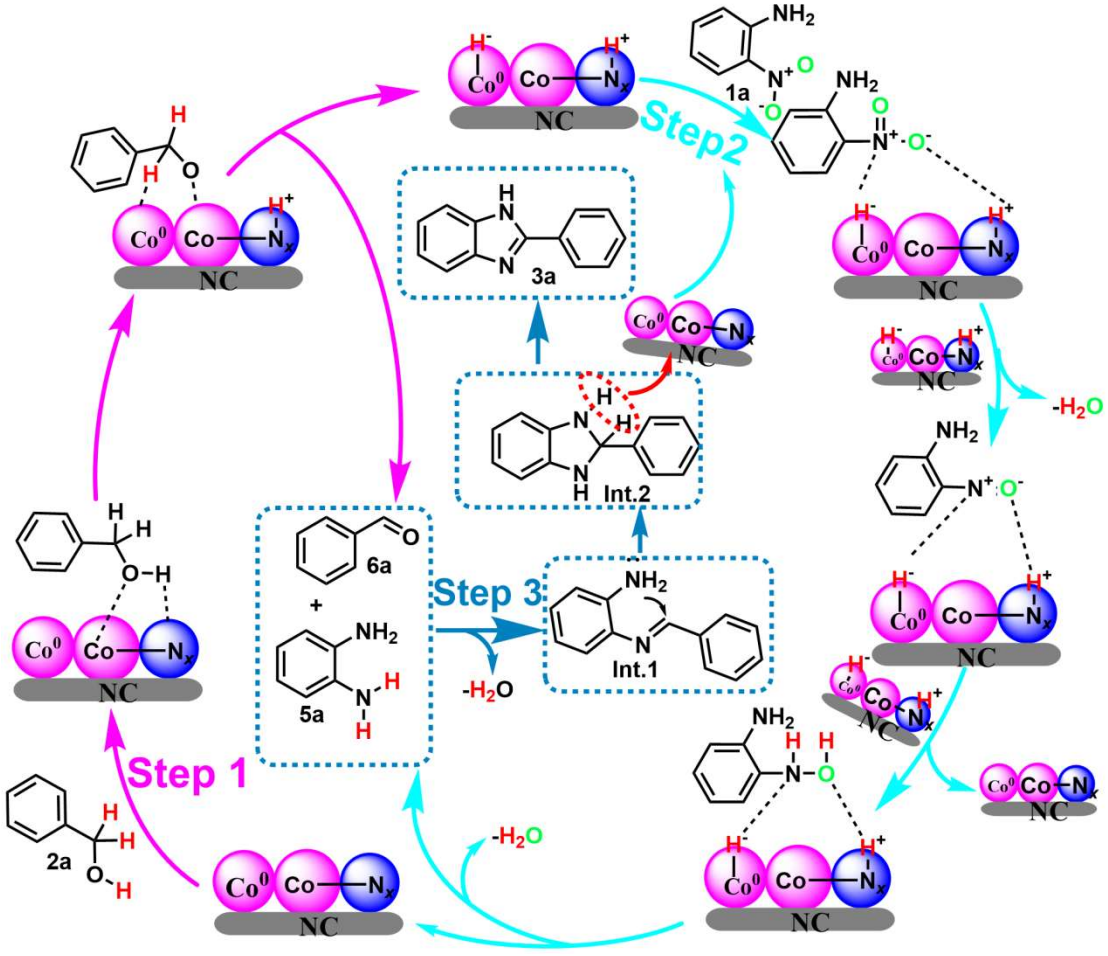

Fig. 16 Possible mechanism of hydrogen transfer-coupling reaction of *o*-nitroaniline (**1a**) and benzyl alcohol (**2a**) over Co/CN_x-700 catalyst.

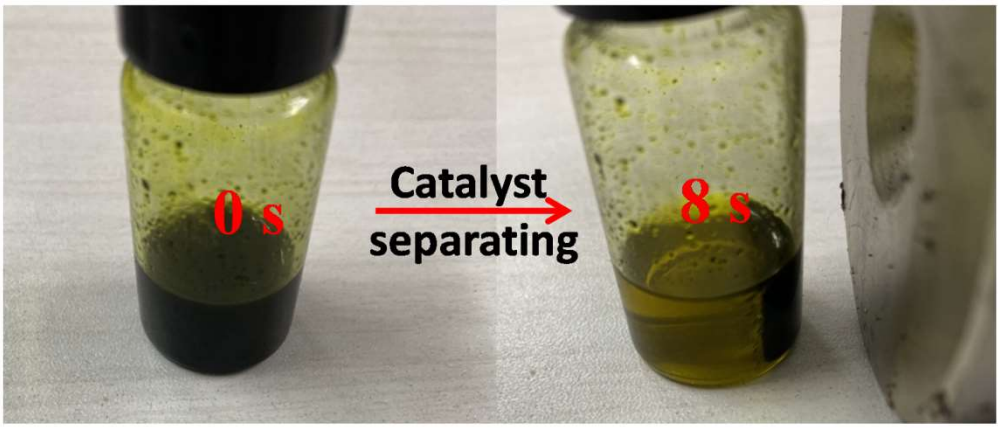

Fig. S17 Magnetic separation of the Co-CN_x-700 catalyst after the reaction.

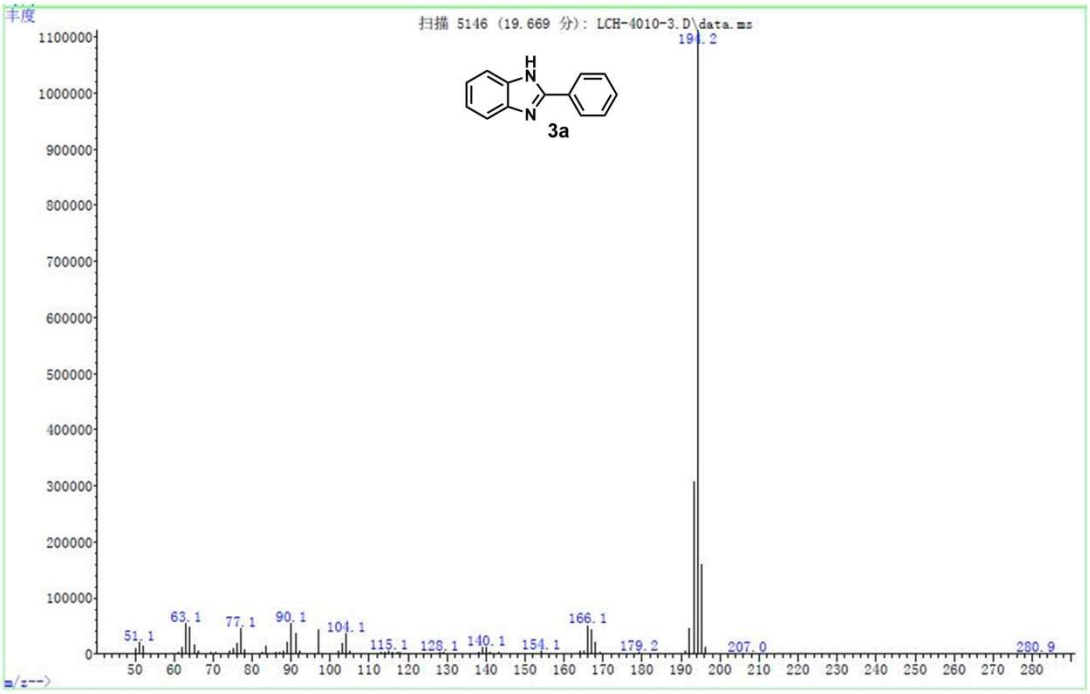

Fig. S18 MS spectrum of **3a**. Abundance versus m/z, scan (5146) at 19.669 min.

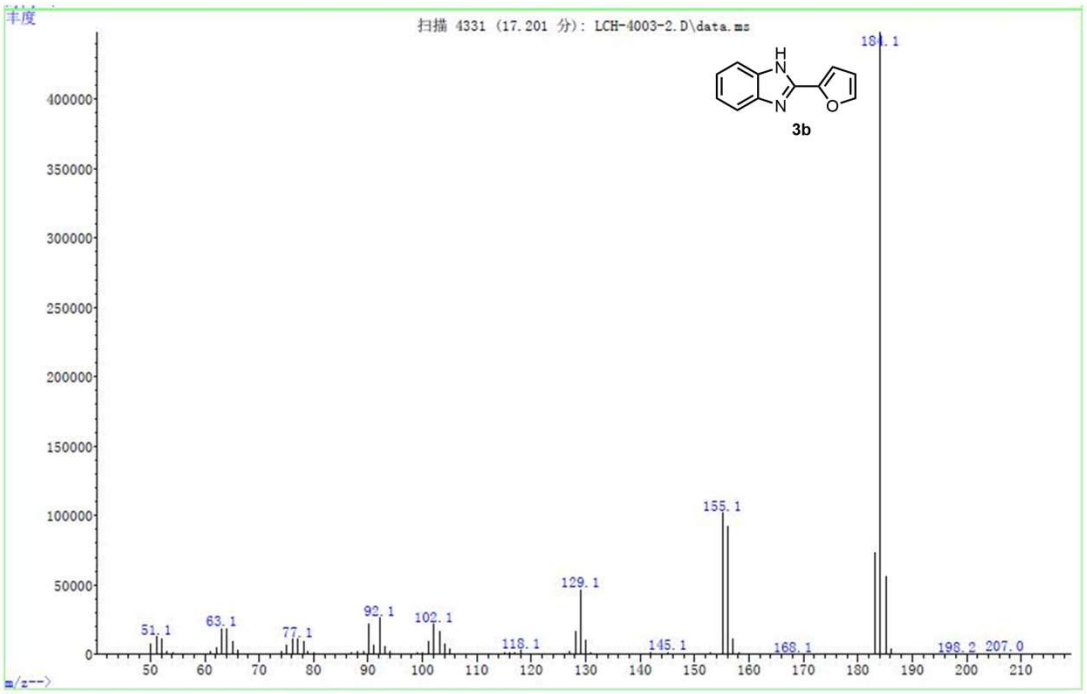

Fig. S19 MS spectrum of **3b**. Abundance versus m/z, scan (4331) at 17.201 min.

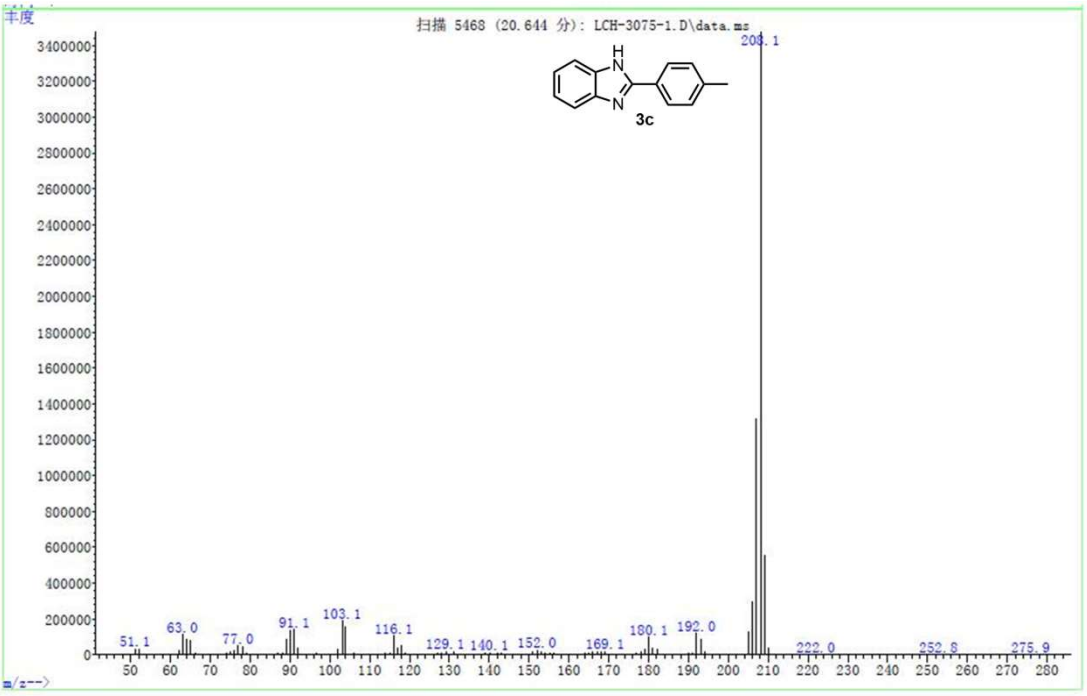

Fig. S20 MS spectrum of **3c**. Abundance versus m/z, scan (5468) at 20.644 min.

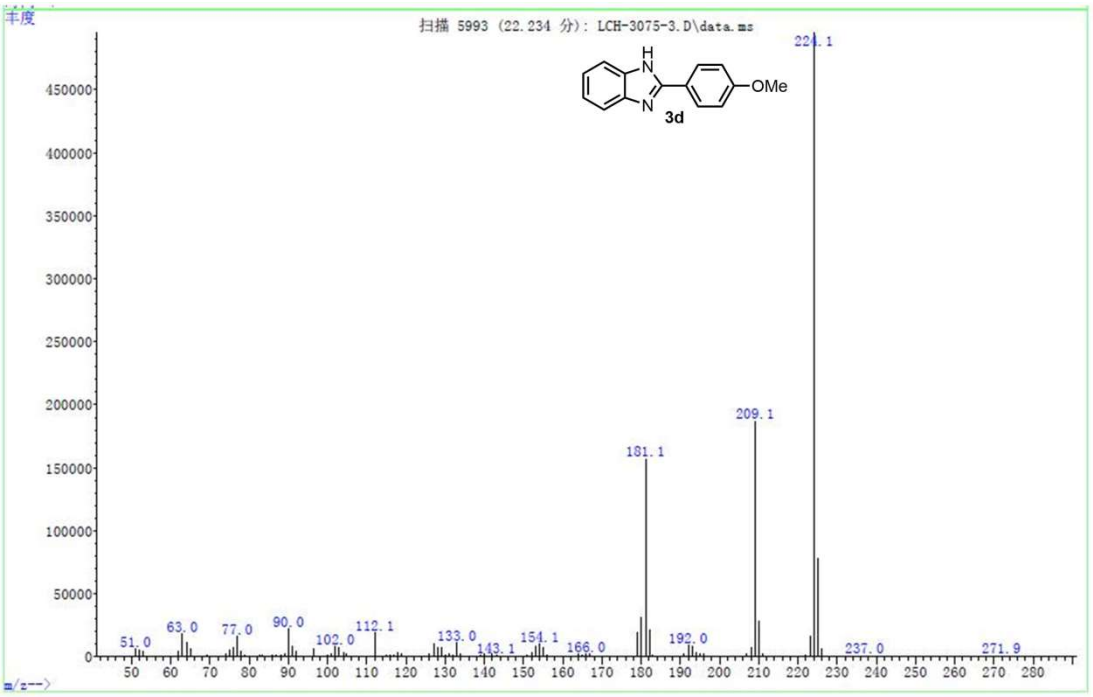

Fig. S21 MS spectrum of **3d**. Abundance versus m/z, scan (5993) at 22.234 min.

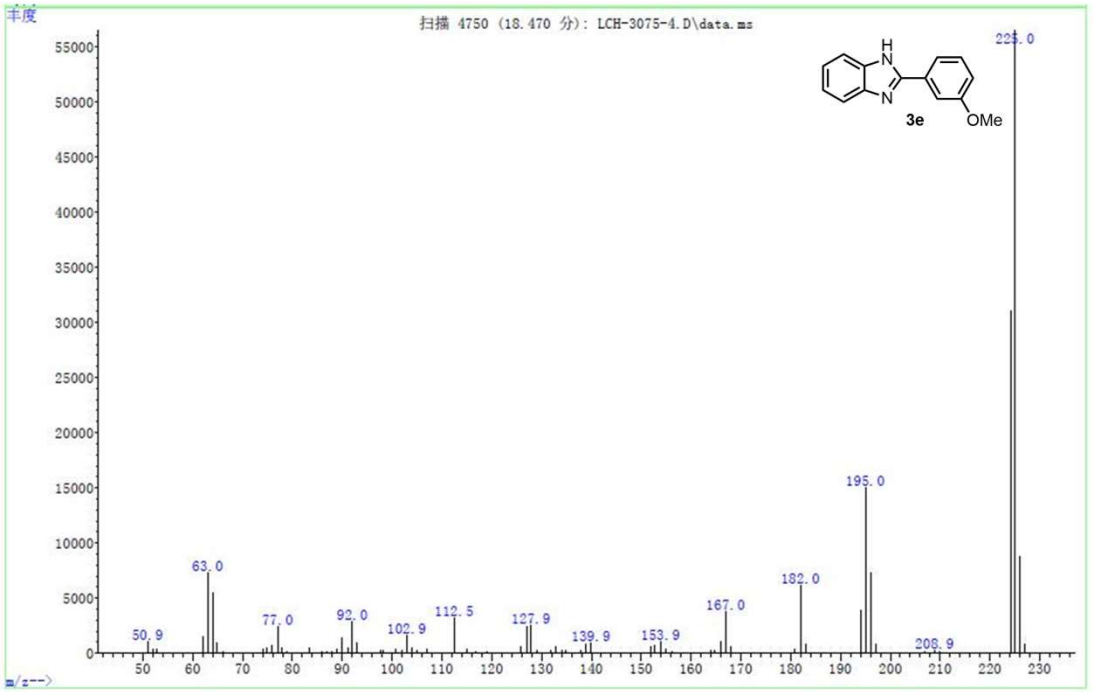

Fig. S22 MS spectrum of **3e**. Abundance versus m/z, scan (4750) at 18.470 min.

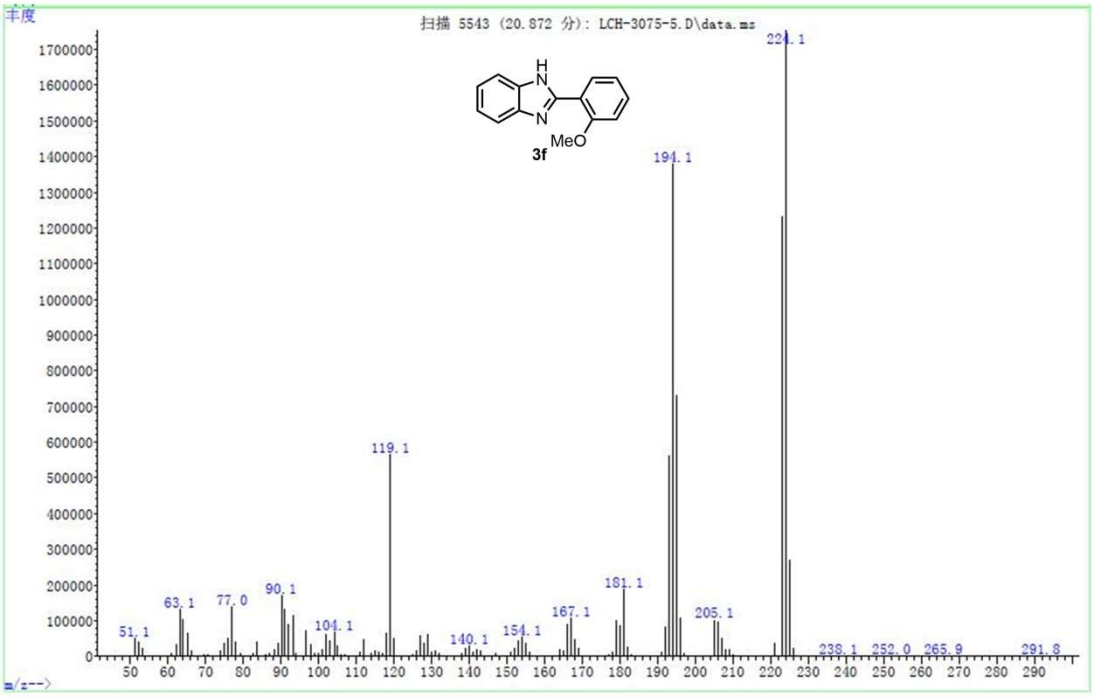

Fig. S23 MS spectrum of **3f**. Abundance versus m/z, scan (5543) at 20.872 min.

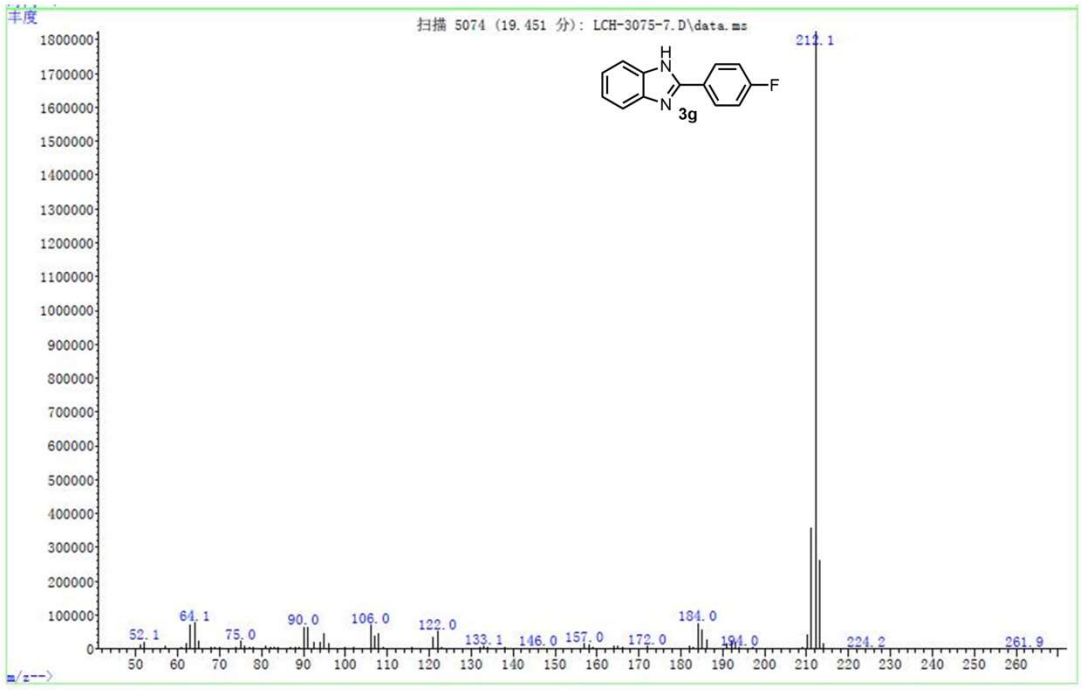

Fig. S24 MS spectrum of **3g**. Abundance versus m/z, scan (5074) at 19.451 min.

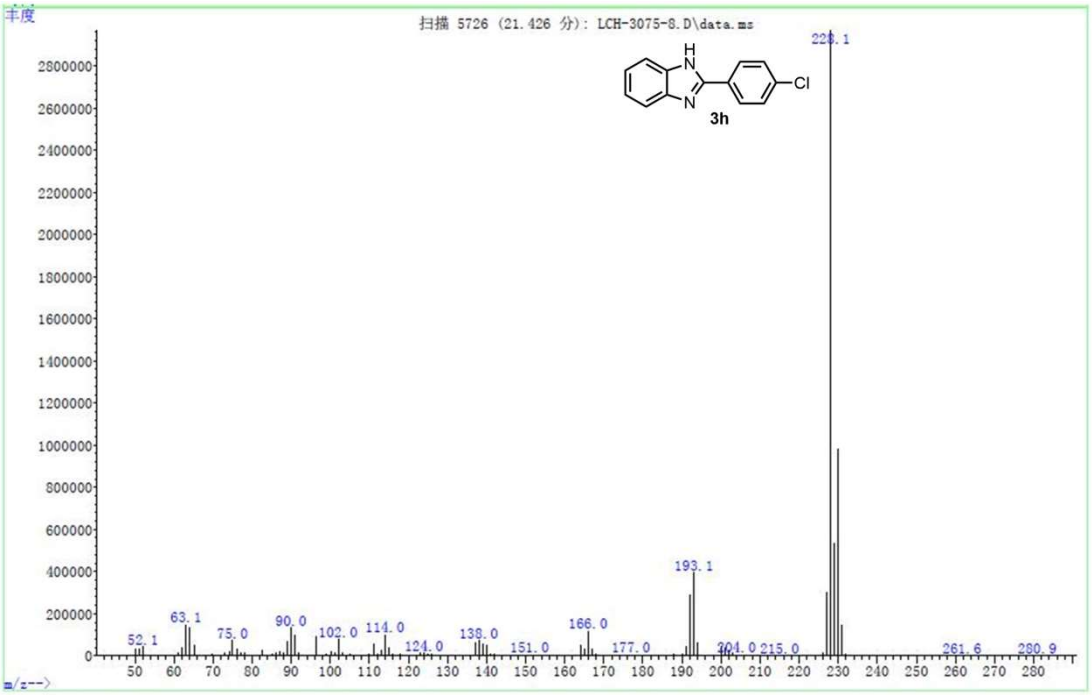

Fig. S25 MS spectrum of **3h**. Abundance versus m/z, scan (5726) at 21.426 min.

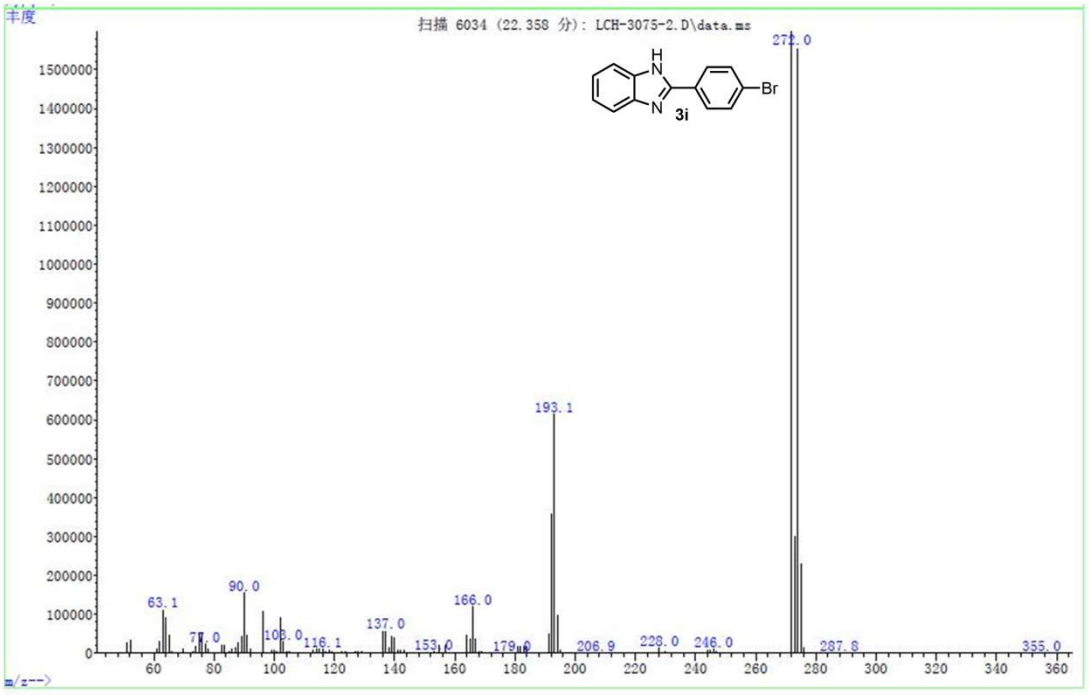

Fig. S26 MS spectrum of **3i**. Abundance versus m/z, scan (6034) at 22.358 min.

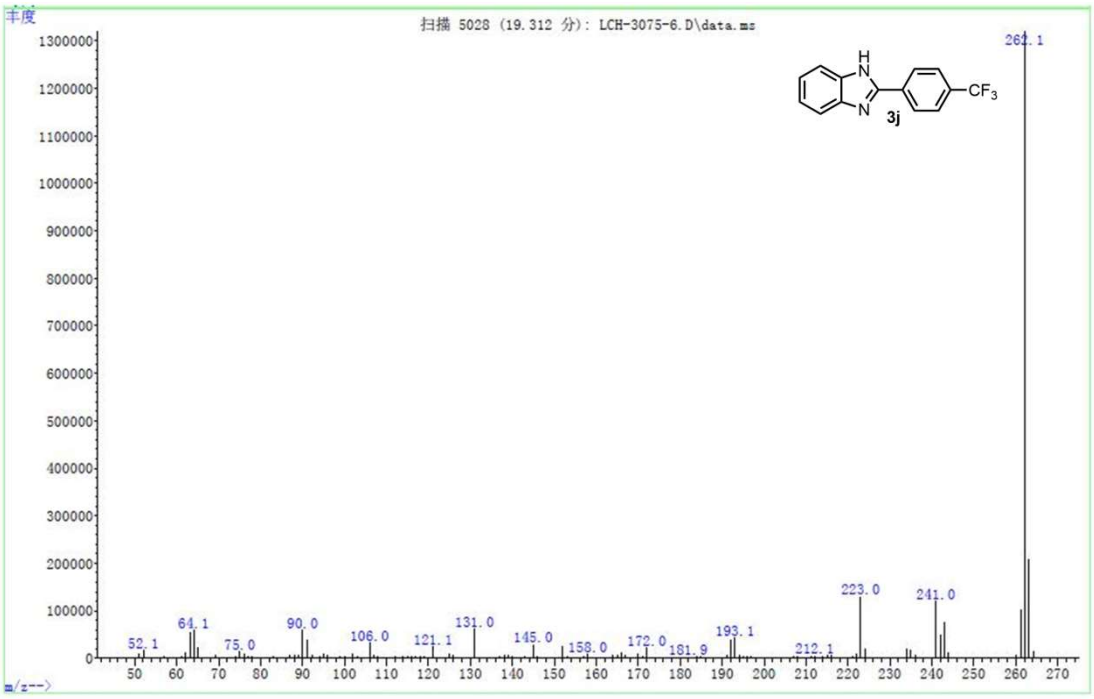

Fig. S27 MS spectrum of **3j**. Abundance versus m/z, scan (5028) at 19.312 min.

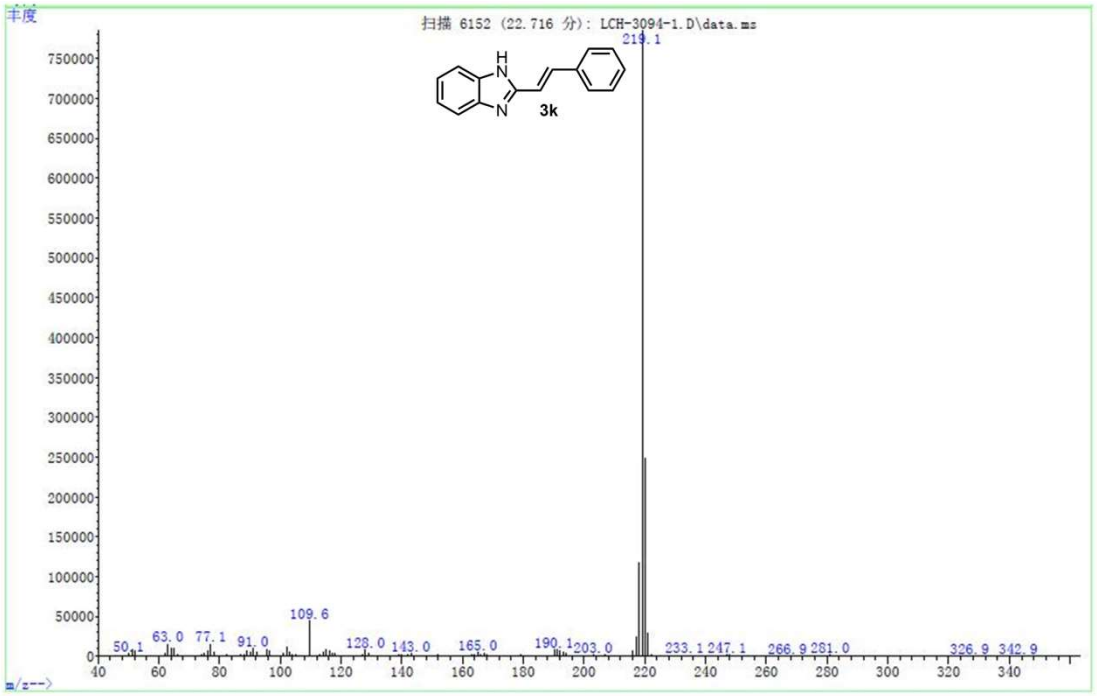

Fig. S28 MS spectrum of **3k**. Abundance versus m/z, scan (6152) at 22.716 min.

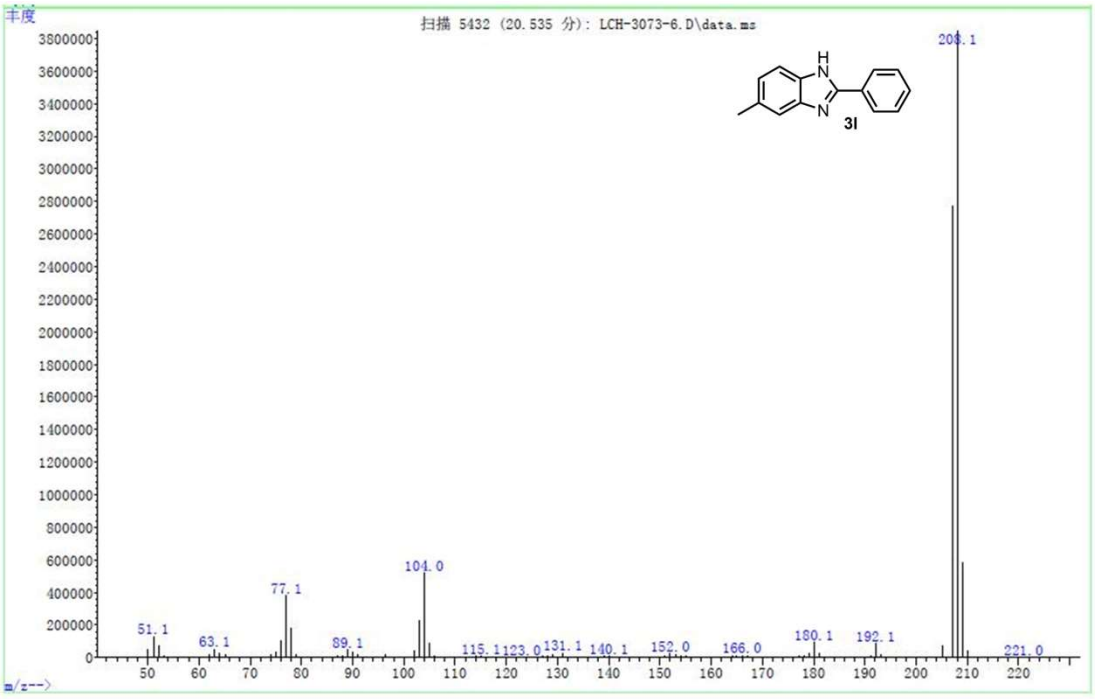

Fig. S29 MS spectrum of **3l**. Abundance versus m/z, scan (5432) at 20.535 min.

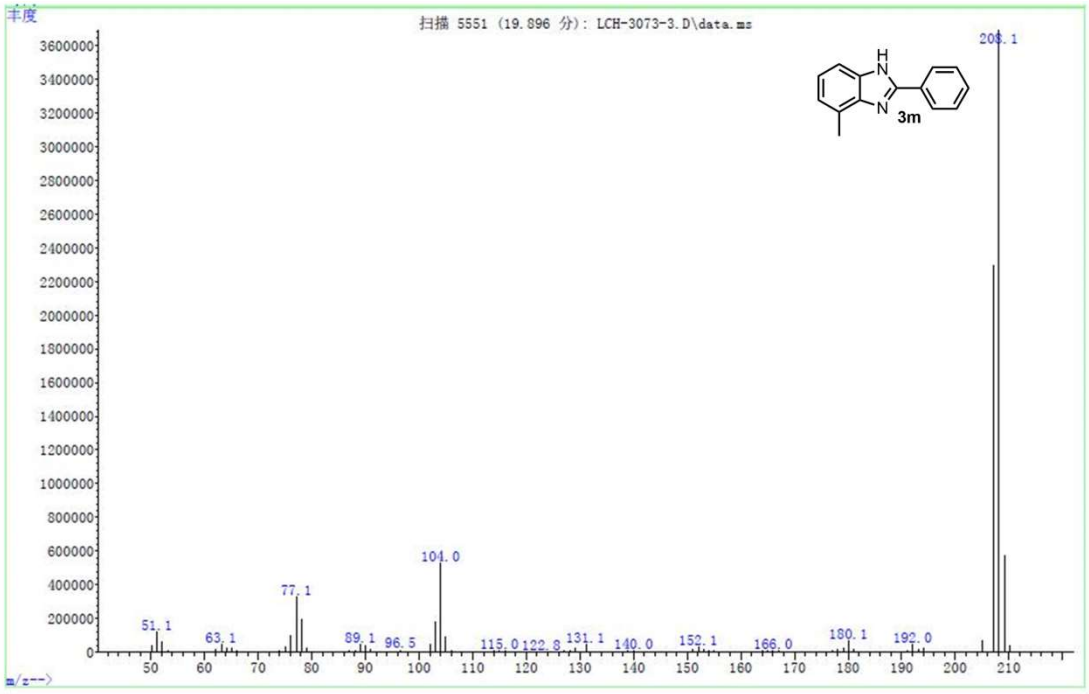

Fig. S30 MS spectrum of **3m**. Abundance versus m/z, scan (5551) at 19.896 min.

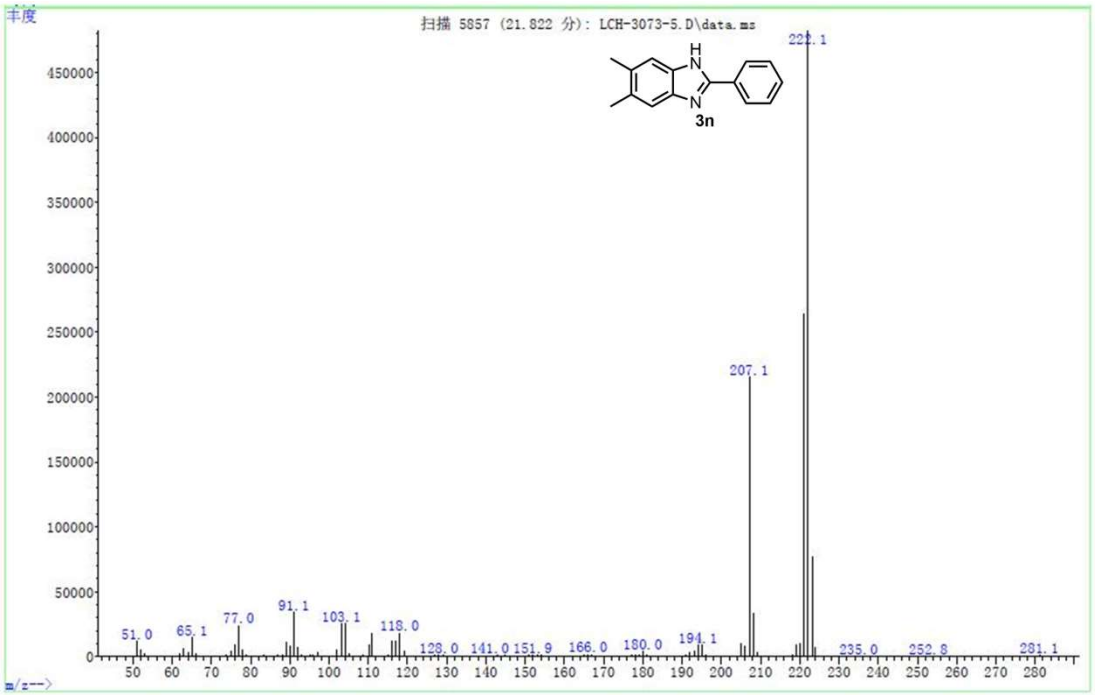

Fig. S31 MS spectrum of **3n**. Abundance versus m/z, scan (5857) at 21.822 min.

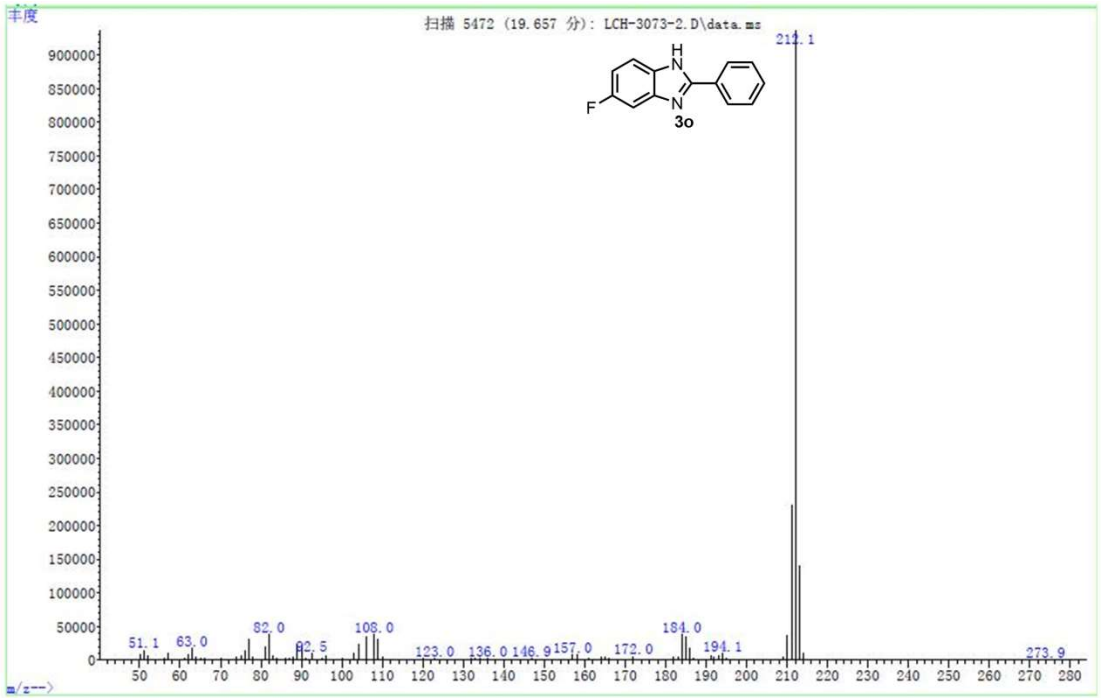

Fig. S32 MS spectrum of **3o**. Abundance versus m/z, scan (5472) at 19.657 min.

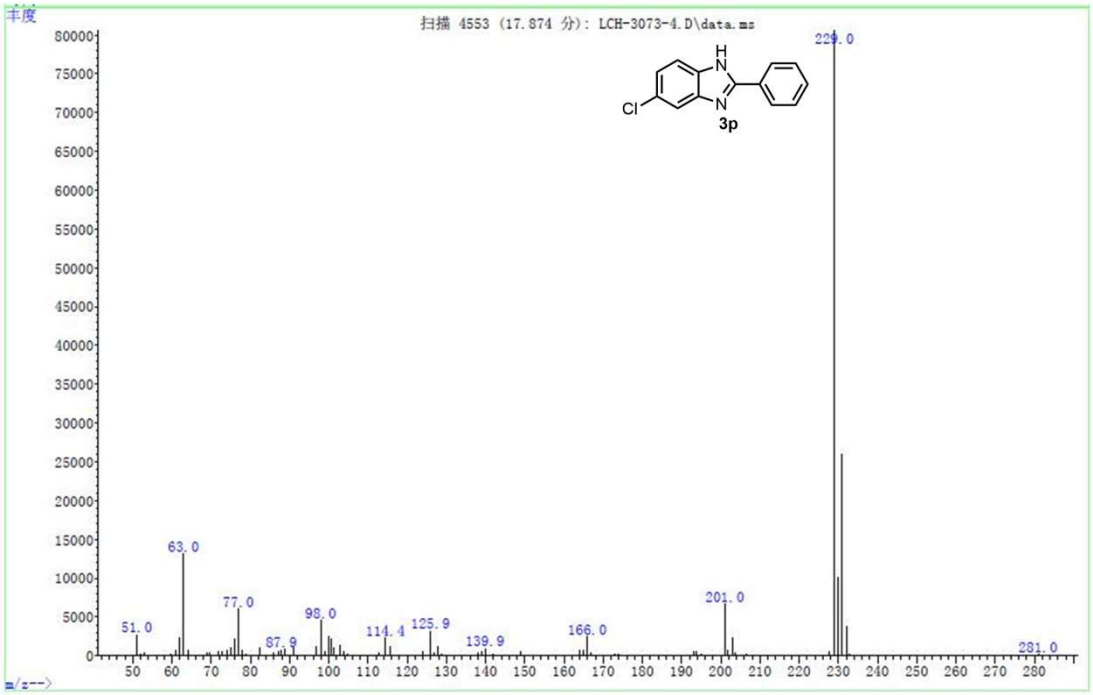

Fig. S33 MS spectrum of **3p**. Abundance versus m/z, scan (4553) at 17.874 min.

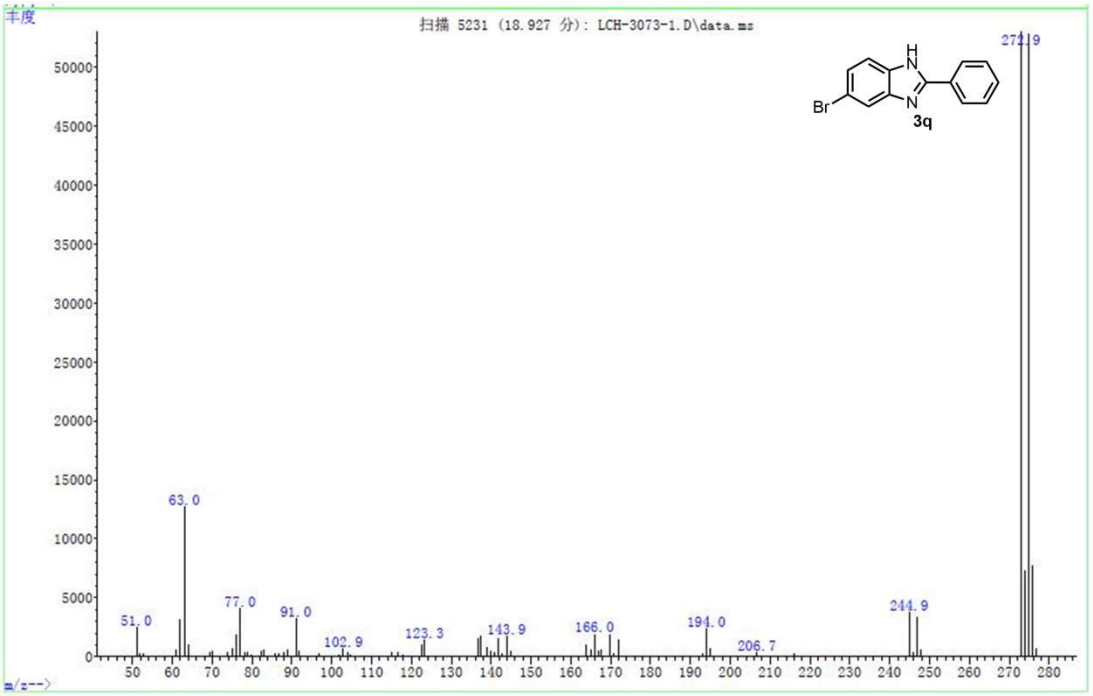

Fig. S34 MS spectrum of **3q**. Abundance versus m/z, scan (5231) at 18.927 min.

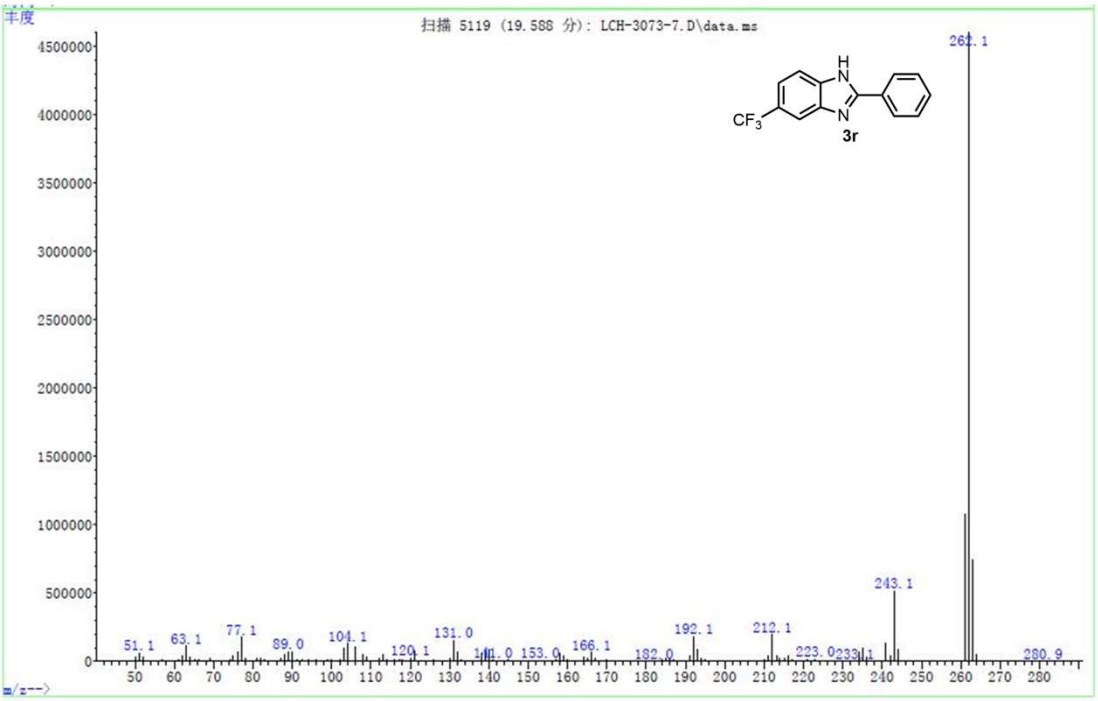

3r

Fig. S35 MS spectrum of **3r**. Abundance versus m/z, scan (5119) at 19.566 min.

References

[S1] B. Djukic, T. Seda, S. I. Gorelsky, A. J. Lough, M. T. Lemaire, *Inorg. Chem.* **2011**, *50*, 7334–7343.

[S2] S. Das, S. Mallick, S. D. Sarkar, *J. Org. Chem.* **2019**, *84*, 12111-12119.

[S3] G. Li, J. Wang, B. Yuan, D. Zhang, Z. Lin, P. Li, H. Huang, *Tetrahedron Let.* **2013**, *54*, 6934-6936.

[S4] R. R. Putta, S. Chun, S. H. Choi, S. B. Lee, D.-C. Oh, S. Hong, *J. Org. Chem.* **2020**, *85*, 15396-15405.

[S5] T. B. Nguyen, L. Ermolenko, A. Al-Mourabi, *Synthesis* **2015**, *47*, 1741-1748.

[S6] Z. Sun, G. Bottari, K. Barta, *Green Chem.* **2015**, *17*, 5172-5181.

[S7] T. Fukutake, K. Wada, H. Yu, S. Hosokawa, Q. Feng, *Mol. Catal.* **2019**, *477*, 110550.

[S8] Q. Guan, Q. Sun, L. Wen, Z. Zha, Y. Yang, Z, Wang, *Org. Biomol. Chem.* **2018**, *16*, 2088.

[S9] H. Yu, K. Wada, T. Fukutake, Q. Feng, S. Uemura, K. Isoda, T. Hirai, S. Iwamoto, *Catal. Today*, **2021**, *375*, 410-417.

[S10] L. Tang, X. Guo, Y. Yang, Z. Zha, Z. Wang, *Chem. Commun.* **2014**, *50*, 6145.

[S11] J. Chen, S. Huang, J. Lin, W. Su, *Appl. Catal. A Gen.* **2014**, *470*, 1-7.

[S12] F. Feng, J. Ye, Z. Cheng, X. Xu, Q. Zhang, L. Ma, C. Lu, X. Li, *RSC Adv.* **2016**, *6*, 72750.